NANO: Brief Reports and Reviews
Vol. 10, No. 5 (2015) 1550067 (10 pages)

DOI: 10.1142/S1793292015500678

World Scientific
www.worldscientific.com

Structure of MnO_x/TiO_2 Catalysts and Their Catalytic Performance in the Gas-Phase Oxidation of *o*-Dichlorobenzene

Wenrui Zhang*,†,‡, Aidong Tang§, Dabin Ren§, Hui Xiang§, Zhiqiang Yu*, Guoying Sheng* and Jiamo Fu*

*State Key Laboratory of Organic Geochemistry
Guangdong Key Laboratory of Environment and Resources
Guangzhou Institute of Geochemistry, Chinese Academy of Sciences
Guangzhou 510640, P. R. China

†University of the Chinese Academy of Sciences
Beijing 100049, P. R. China

§School of Chemistry and Chemical Engineering
Central South University, Changsha 410083, P. R. China
‡wenrui.mao@163.com

Received 15 December 2014
Accepted 27 February 2015
Published 19 May 2015

The influence of structure of MnO_x/TiO_2 catalysts and their catalytic oxidation of *o*-dichlorobenzene were examined in this study. MnO_x/TiO_2 catalysts were characterized by X-ray diffractometer (XRD), thermogravimetry-differential thermal analysis (TG-DTA), TEM, X-ray photoelectron spectrum (XPS) and FTIR for NH_3 adsorption techniques. Experimental results indicated that the MnO_x/TiO_2 catalyst prepared from manganese nitrate possessed the highest catalytic activity with a gas hourly space velocity (GHSV) of 14,500 h^{-1}. This activity may be due to a large amount of surface Mn_2O_3 species, the strong Brönsted and Lewis acidity and the combined TiO_2 phases. Additionally, a possible reaction model from *o*-dichlorobenzene oxidation over MnO_x/TiO_2 catalyst was suggested based on the analysis.

Keywords: *o*-dichlorobenzene; catalytic oxidation; catalyst; MnO_x/TiO_2.

1. Introduction

Incineration of wastes is expected to be more appealing as it reduces the mass and volume of wastes and produces energy.[1] However, the combustion processes have the huge drawback of producing many organic products of incomplete combustion; these organic products can be named as dioxins. They are all environmentally persistent organic pollutants, very toxic and carcinogenic.[2–5] Therefore, in order to fix the problem of the atmospheric mission of these chlorinated volatile organic compounds (Cl-VOCs), strict emission limits have been imposed by environmental legislation. Techniques such as thermal incineration, adsorption and so on,[6] have been developed for solving this trouble of atmospheric release of Cl-VOCs. Thermal incineration

‡Corresponding author.

needs temperatures higher than 850°C. Thermal treatment is quite expensive and may also lead to emission of by-products, such as dioxins, dibenzofurans, etc due to incomplete combustion.[7] For the adsorption technique, a special new kind of carbonaceous materials[8] was applied for Cl-VOCs removal recently. Despite the success of adsorption and thermal incineration, there is still a need for research on techniques, which are both economically more favorable and truly destroy the pollutants rather than merely remove them for recycling elsewhere in nature. The catalytic destruction of Cl-VOC to CO_x, H_2O and HCl/Cl_2 appears very promising in this context.[1] In order to further catalytic oxidize Cl-VOC, some promoters such as ozone, are usually added to promote the catalytic performance of the catalysts.[9,10] However, the promotion effect of ozone disappeared at high temperature (above 200°C) for the decomposition of ozone. Therefore, an effective catalyst itself is the key to flue gas treatment.

In recent years, manganese oxides have been reported to be among the most efficient transition-metal oxide catalysts for catalytic disposal of pollutants.[11] They have been widely used in selective catalytic reduction of NO_x with NH_3,[12–14] CO,[15] VOC[16,17] and Cl-VOCs[18,19] oxidation since they contain various types of labile oxygen, which are necessary to complete a catalytic cycle.[20]

Most of supported Mn-based catalysts were prepared by the impregnation method using manganese nitrate (MN) or manganese acetate (MA) as a raw material. The kinds of Mn precursors, which induce different oxidation states during preparation of catalysts, have been reported affecting the catalyst activities in several systems. It is generally believed that the efficiency and selectivity of reaction depends on the dispersion and oxidation patterns of MnO_x, and the order catalytic activity of MnO_x is $MnO_2 > Mn_5O_8 > Mn_2O_3 > Mn_3O_4$.[21] Many efforts have been devoted to investigate the effects of different phases of MnO_x on low-temperature SCR. Kapteijn *et al.*[22] reported that MA precursor results in better dispersion of MnO_x on alumina and higher catalytic activity than MN at 100–180°C. However, Pena *et al.*[23] claimed that the MnO_x/TiO_2 catalyst prepared from MN showed a better performance than that prepared from the MA precursor at 100–200°C. Li *et al.*[24] pointed that the higher low-temperature activity of MnO_x/TiO_2 from MA was attributed to the higher surface Mn concentration and the surface Mn_2O_3 species. Tang *et al.*[25] made a distinction that the excellent low temperature catalytic activity of MnO_x catalysts was mainly due to their amorphous Mn_3O_4 phase. However, few results about the role of the MnO_x for catalytic oxidation of Cl-VOC on MnO_x/TiO_2 have been reported. This work is mainly focused on the effect of MnO_x structure of MnO_x/TiO_2 catalysts for *o*-DCB removal. It will help us to better understand how the degradation of *o*-DCB was affected over the supported MnO_x/TiO_2 catalysts.

2. Experimental

2.1. *Catalysts preparation*

The MnO_x/TiO_2 catalysts are prepared from different manganese compounds, MA, MN and manganese carbonate (MC), and the catalysts could be denoted as MN-MnO_x/TiO_2, MA-MnO_x/TiO_2 and MC-MnO_x/TiO_2, respectively. TiO_2 used in this study was Hombikat UV 100 from Sachtleben Chemie.[26] As determined by N_2 adsorption, it had a specific surface area of 309 m^2/g, a pore volume of 0.37 cm^3/g, a pore diameter of 4.5 nm. An amount of 80 mL of distilled water was added to a 250 mL beaker containing appropriate amount of MN($Mn(NO_3)_2$ 50% solution) or MA($Mn(CH_3COO)_2 \cdot 4H_2O$) or MC ($MnCO_3$) precursor with stirring, 10.0 g TiO_2 support was added consecutively, and the mixture was stirred at 80°C until the water was evaporated. The paste obtained was dried overnight at 105°C and was crushed into fine powder named MnO_x/TiO_2 precursors. Finally, the precursors were calcined at 500°C for 6 h to obtain MnO_x/TiO_2 composite catalysts. At the same time, MN-MnO_x/TiO_2 catalysts with different atomic ratios of Mn/Ti (1:10, 1:8, 1:6, 1:4, 2:4, 3:4, 4:4) and different calcination temperature (200°C, 300°C, 400°C, 500°C, 600°C) were prepared by following the steps above.

2.2. *Characterization of catalyst*

The phase structure of catalysts were performed on a D8-ADVANCE X-ray diffracto-meter (XRD) with CuKα radiation (CuKα = 0.15406 nm). The morphology of the samples was observed by Tecnai $G^2$20 transmission electron microscope (TEM). Thermal decomposition of catalyst precursors were monitored by thermogravimetry/differential thermal analysis (TG-DTA) at a heating rate of 10°C/min up to 800°C. X-ray photoelectron spectrum (XPS) measurements were used to determine the atomic

concentration and the state of the elements on catalyst surface with a Thermo ESCALAB 250 with Al Kα ($h\nu = 1486.6$ eV) X-rays. The concentration of Mn and Ti on the surface of the samples was calculated from the integral of peak areas of the XPS data divided by each sensitivity factor of the element. The FTIR spectra during NH_3 adsorption experiment was recorded with a Nicolet Nexus 670 spectrometer, collecting 100 scans at a spectral resolution of 2 cm^{-1}. The powdered sample was placed in a cell which allows thermal treatments in vacuum or in a controlled atmosphere. In the cell, all samples were treated at 150°C in air for 1 h, cooled down to room temperature in air and out gassed at room temperature for 1 h. NH_3 was then admitted by opening for 5 min the valve of the vessel containing the substance at 25°C. Desorption were then performed by evacuation for 30 min at room temperature. The powdered samples were compressed into thin self-supporting discs of about 0.1 mm thick. Data are reported as difference spectra obtained by subtracting the spectrum of the sample before the admission of NH_3.

2.3. *Catalytic activity measurement*

The catalytic oxidation of *o*-DCB was carried out in a self-designed fixed-bed reactor under atmospheric pressure of 150–300°C (Fig. 1).

The *o*-DCB containing feed stream to the reactor was carried by air and controlled by a flow controller. The total flow rate through the reactor was set at 150 mL/min, corresponding to a gas hourly space velocity (GHSV) of 14,500 h^{-1}. The concentration of *o*-DCB in air was 3% and the O_2/*o*-DCB molar ratio was 6.8:1 before reaction. Oxygen was excess to insure complete oxidation of *o*-DCB. Acetone was used as the absorption solution, the *o*-DCB concentration difference between bottles 1 and 2 was conducted as the evaluation standard of catalytic performance. The final products of CO and CO_2during *o*-DCB catalytic oxidation have been detected by gas chromatography (GC) and absorbed by exhaust collection device. CO and CO_2 during *o*-DCB catalytic oxidation have been detected by gas chromatography (GC-4004) equipped with thermal conductivity detector. A TDX-01 column (1 m × 2.5 mm, i.d.) was used to determine CO and CO_2. Helium was used as the carrier gas at a flow rate of 10 mL/min. The temperature of the column and detector of GC were setup as 60°C and 100°C, respectively. The retention time of CO and CO_2 was 8.6 min and 24.8 min respectively (see Fig. 2). Compared with the highly toxic Cl-VOC which are carcinogenic and environmentally persistent, the products are lower toxicity and harmful.[7]

As the catalyst powders could not easily be fixed in the reactor, ceramic honeycombs were used as carrier. Catalyst powders were dispersed in deionized water with mass ratio of 1:40, and then they were loaded inside the pore of ceramic honeycombs by impregnation. Finally, these ceramic honeycombs were dried at 110°C overnight for catalytic activity test without further treatment. After 60 min reaction at each temperature, quantitative analysis of *o*-DCB was continuously performed by GC-4004 equipped with flame ionization detector and thermal conductivity detectors. During the *o*-DCB analysis, the temperature of the column and detector of GC with nitrogen as carrier gas were setup as 250°C and 260°C, respectively. The type of column used for separation is GDX-101 and the pressure for column, H_2, N_2 and O_2 were 0.08, 0.05, 0.3 and 0.2 MPa, respectively. *o*-DCB conversion efficiency was obtained by the following equation:

$$o\text{-DCB conversion} = ([o\text{-DCB}]_{\text{bottle 1}} - [o\text{-DCB}]_{\text{bottle 2}})/[o\text{-DCB}]_{\text{bottle 1}} \times 100\%. \quad (1)$$

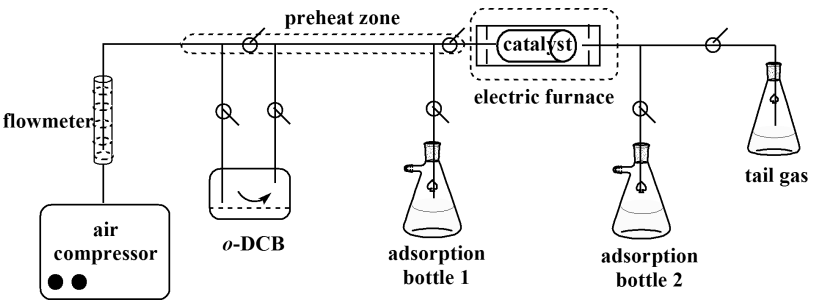

Fig. 1. Schematic diagram of the experimental apparatus.

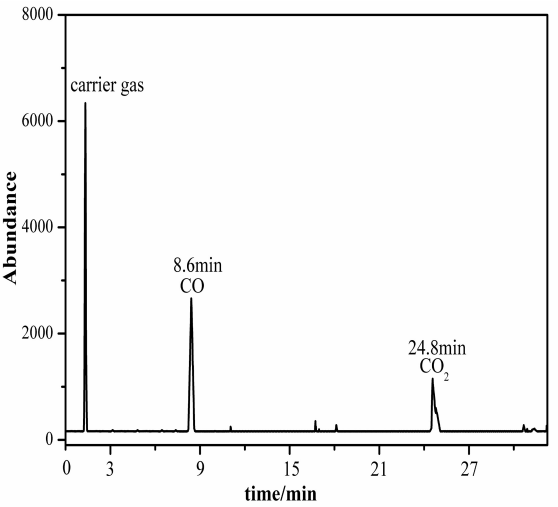

Fig. 2. The chromatograms of the products: CO and CO_2.

3. Results and Discussion

3.1. *Catalytic testing*

The results of *o*-DCB conversion efficiency as a function of temperature over the three catalysts prepared by three manganese compounds are shown in Fig. 3. Pure TiO_2 or ceramic honeycomb was also presented for comparison. It was clear that pure TiO_2 or ceramic honeycomb showed no catalytic activity. MN-MnO_x/TiO_2 performed a best catalytic capacity in all catalysts. The conversion efficiencies of *o*-DCB were all above 60% at the temperature ranging from 150°C to 300°C, and its activity was enhanced slowly with increasing temperature. About

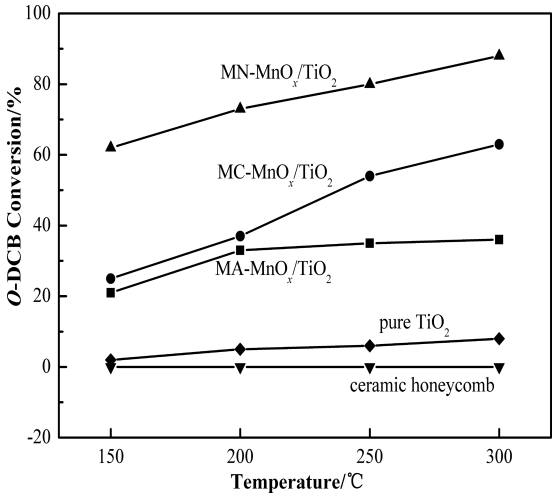

Fig. 3. Catalytic activities of MnO_x/TiO_2 prepared from different manganese compounds.

Table 1. The catalytic oxidations of *o*-DCB over MN-MnO_x/TiO_2 catalysts with different ratio of Mn/Ti at 500°C.

	o-DCB conversion efficiency (%)			
Samples	150°C	200°C	250°C	300°C
Mn/Ti = 1:4	60	73	80	88
Mn/Ti = 2:4	12	25	29	33
Mn/Ti = 3:4	21	26	37	47
Mn/Ti = 4:4	33	38	35	24

90% of *o*-DCB could be decomposed with MN-MnO_x/TiO_2 as catalyst at 300°C with a GHSV of 14,500 h^{-1}. However, the conversion efficiencies of *o*-DCB over MA-MnO_x/TiO_2 and MC-MnO_x/TiO_2 were below obviously compared with MN-MnO_x/TiO_2 under the same condition.

Then, the preparation parameters such as temperature of calcination and Mn content had been evaluated for MN-MnO_x/TiO_2. The catalytic oxidations of *o*-DCB over MN-MnO_x/TiO_2 catalysts prepared with different ratio of Mn/Ti at 500°C and different temperature of calcination are listed in Tables 1 and 2, respectively. About atomic ratio of Mn/Ti of MnO_x/TiO_2 catalysts, we made reference from Tian[27] because the main component of the catalyst was similar. Except the four groups of Mn:Ti ratio (1:4, 2:4, 3:4 and 4:4), we designed additionally the Mn:Ti ratio of 1:10, 1:8 and 1:6. From the results of catalytic activity, the Mn:Ti ratio before 1:4 was not good. So, the corresponding data were not shown here. As listed in Table 1, the loading of Mn had significant effect on the activity of MN-MnO_x/TiO_2. *o*-DCB conversion efficiency decreased with the increase of Mn loading, and the activity of MN-MnO_x/TiO_2 reached the highest value when the ratio of Mn/Ti was 1:4. The further increase of Mn loading amount would lead to the decrease of *o*-DCB conversion efficiency maybe due to the sintering effect.[28] This effect will cause a

Table 2. The catalytic oxidations of *o*-DCB over MN-MnO_x/TiO_2 catalysts calcined at different temperatures.

	o-DCB conversion efficiency (%)			
Samples	150°C	200°C	250°C	300°C
MN-MnO_x/TiO_2-200	42	48	49	51
MN-MnO_x/TiO_2-300	33	31	43	39
MN-MnO_x/TiO_2-400	23	22	27	28
MN-MnO_x/TiO_2-500	60	73	80	88
MN-MnO_x/TiO_2-600	14	18	16	11

decrease in the number of surface metal atoms per unit mass of metal and therefore decreases the number of active sites of the catalyst.[29]

It can be seen from Table 2 that the MN-MnO_x/TiO_2 calcined at 500°C can perform most efficiently in all samples. The differences resulted from the activities may get an explanation from the active MnO_x species from the TG-DTA profiles. Therefore, the catalysts prepared with Mn/Ti ratio of 1:4 at 500°C were selected to be investigated.

3.2. *Characterization of catalysts*

The XRD patterns of origin TiO_2 powders and catalysts prepared from three manganese compounds are shown in Fig. 4. Two messages about MnO_x/TiO_2 catalysts were obtained from XRD chart. First, different manganese oxides formed in the three catalysts. For MA-MnO_x/TiO_2, it can be seen that Mn_3O_4 (PDF card 24-0734) was the only manganese oxides observed on the surface. For MC-MnO_x/TiO_2 compared with MA-MnO_x/TiO_2, the oxidation state of MnO_x changed: besides Mn_3O_4, several new diffraction peaks that appeared were attributed to Mn_2O_3 (PDF card 41-1442). For MN-MnO_x/TiO_2, there were also some peaks corresponded to Mn_2O_3 and Mn_3O_4, but the intensities of Mn_3O_4 peaks was very weak. It can be seen that the intensity of Mn_2O_3 in MN-MnO_x/TiO_2 ($Mn_2O_3\% = 25.5\%$) was stronger than that in MC-MnO_x/TiO_2 ($Mn_2O_3\% = 23.5\%$). Some MnO_x peaks were vague because it is covered by strong TiO_2 peaks. Second, there were two phases for the origin of TiO_2 powders. Besides the typical diffraction peak characteristic of anatase ($2\theta = 25.3°$) was observed, some peaks assigned to the rutile phases ($2\theta = 27.5°$) were also detected. So, we can see that the phase of TiO_2 of three catalysts was a mixture of anatase and rutile. Thus, there were two factors on the high catalytic activity for MN-MnO_x/TiO_2 according to the results of *o*-DCB conversion efficiency: on one hand, it can be concluded that the MnO_x for MN-MnO_x/TiO_2 could be considered as mixed oxides of Mn_2O_3 and Mn_3O_4, and the majority was Mn_2O_3 that played a crucial role in the reaction; on the other hand, we can speculate that there may be a kind interaction between MnO_x and carrier. It had been analyzed that TiO_2 in anatase phase and rutile phase would be a good carrier,[30] which contributed to a better dispersion of MnO_x. Thus, the combined TiO_2 phase and a large of Mn_2O_3 in MN-MnO_x/TiO_2 might contribute to its high activity. While for catalysts MA-MnO_x/TiO_2 and MC-MnO_x/TiO_2, little Mn_2O_3 would lead to relatively lower activity.

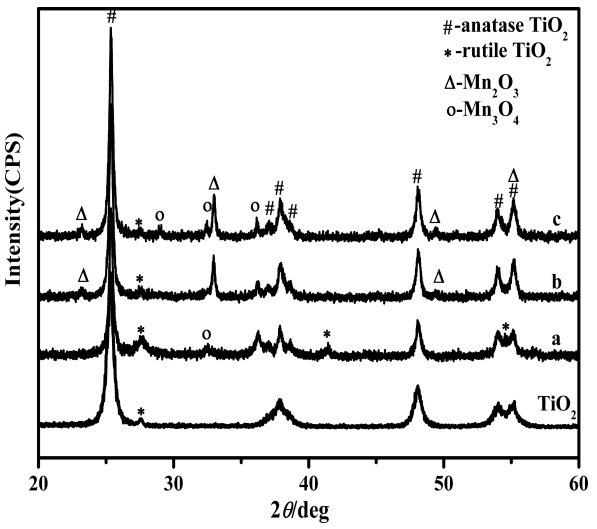

Fig. 4. XRD patterns of catalysts prepared from different manganese compounds: (a) MA-MnO_x/TiO_2, (b) MN-MnO_x/TiO_2, (c) MC-MnO_x/TiO_2.

Thermal analysis results of the MnO_x/TiO_2 precursors are shown in Fig. 5. The weight loss below 150°C was related to the decomposition of physically adsorbed water and surface impurities on these three samples. The curve of MA-MnO_x/TiO_2 in Fig. 5(a) depicts that the endothermic peak stayed at 273°C accompanied with a weight loss on TG curve, was caused by the formation of manganese oxides. No clear weight loss was recorded from 300°C to 800°C on the TG and DTA curve. There was only Mn_3O_4 in the MA-MnO_x/TiO_2 catalyst according to the results of XRD. In contrast, distinct differences were recorded on the TG-DTA curves of MN-MnO_x/TiO_2 and MC-MnO_x/TiO_2. In Fig. 5(b), there were two endothermic peaks located 218°C and 330°C accompanied with a weight loss on TG curve, which may be ascribed to the formation of MnO_x such as MnO_2 or Mn_2O_3 ($2MnO_2 \rightarrow Mn_2O_3 + O$). It can be seen that a slight weight loss at 500°C on the TG and DTA curve was attributed to the decomposition of a few Mn_2O_3 ($3Mn_2O_3 \rightarrow 2Mn_3O_4 + O$).[5] In Fig. 5(c), the endothermic peaks presenting the formation of MnO_x was 265°C and 362°C, respectively, but the peak at 500°C belonging to the decomposition of Mn_2O_3 was stronger than Fig. 5(b). This probably constituted the reason why the amount of Mn_2O_3 on MC-MnO_x/TiO_2 was less than that on MN-MnO_x/TiO_2 according to the results of XRD. Conclusion

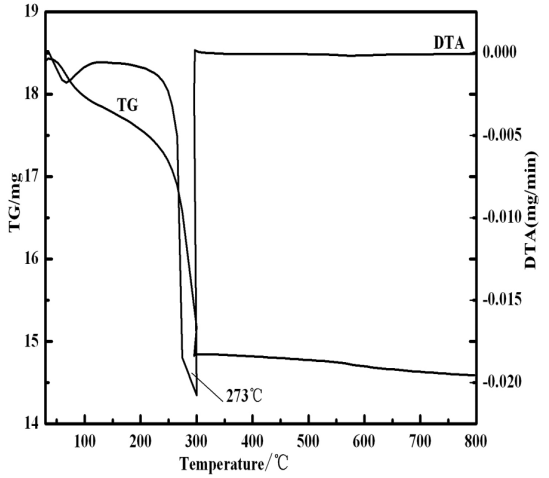

(a)

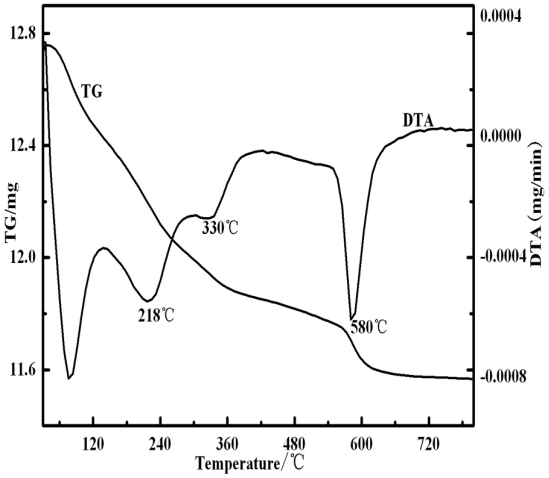

(b)

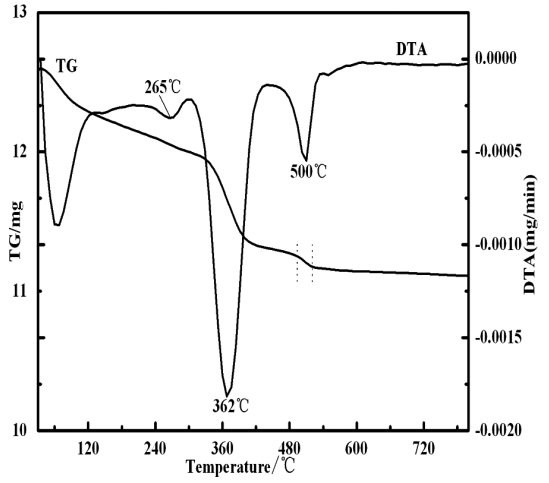

(c)

Fig. 5. TG-DTA profiles of three MnO_x/TiO_2 precursors: (a) MA-MnO_x/TiO_2, (b) MN-MnO_x/TiO_2, (c) MC-MnO_x/TiO_2.

would be drawn that a massive Mn_2O_3 exiting in MN-MnO_x/TiO_2 calcined at 500°C is responsible to its high activity. Besides, the presence of manganese will inhibit the phase transition of TiO_2.[23] So, there was no evidence in the thermal analysis of the phase transition of TiO_2.

TEM images of MnO_x/TiO_2 were obtained in order to get more details about the microstructure of catalysts. Figures 6(a)–6(c) indicated that there were no significant disparities in the morphology of three catalysts. Catalyst particles of MnO_x/TiO_2 had comparatively regular flaky shape with low crystalline and the grain size mainly ranges from 40 nm to 50 nm. It was also shown that the agglomeration of MA-MnO_x/TiO_2 and MC-MnO_x/TiO_2 was more serious due to calcination than MN-MnO_x/TiO_2. The crystals of TiO_2 could be seen while MnO_x could not be seen and the grain size was much bigger than MN-MnO_x/TiO_2, which provides further evidence of lower crystallinity of manganese oxides. From this result, we can infer that the dispersion of manganese oxides on MN-MnO_x/TiO_2 was better than on the other catalysts, which can be the reason for the good catalytic activity of MN-MnO_x/TiO_2.

XPS was used to measure the concentration of the atoms on the surface of MnO_x/TiO_2 catalysts. As shown in Table 3, the concentration of Mn on the surface of MA-MnO_x/TiO_2 was the highest, and the order of Mn/Ti ratio on the surface was MA-MnO_x/TiO_2 > MN-MnO_x/TiO_2 = MC-MnO_x/TiO_2.

It can also be seen that the sequence of the catalytic activity was MN-MnO_x/TiO_2 > MC-MnO_x/TiO_2 > MA-MnO_x/TiO_2. Experimental results revealed that the order of the concentration of Mn in the three samples was not the same as that of their catalytic activity. Though the concentration of Mn in MA-MnO_x/TiO_2 was the highest of all, its catalytic activity among the three was the lowest. It might be because the more serious adhesion of MA-MnO_x/TiO_2 can lead to higher concentration of Mn badly dispersing on the surface, which resulted in the lower catalytic capacity for *o*-DCB.

Figure 7 compares the $Mn2p_{3/2}$ XPS spectra for these three catalysts respectively. The spectrum of MA-MnO_x/TiO_2 (a) showed an asymmetric peak at 641.7 eV which was attributed to Mn_3O_4,[31] consistent with the XRD results that Mn_3O_4 was the only manganese oxide in MA-MnO_x/TiO_2. The MN-MnO_x/TiO_2(b) and MC-MnO_x/TiO_2(c) catalyst showed a symmetric $Mn2p_{3/2}$ peak at 642.57 eV and

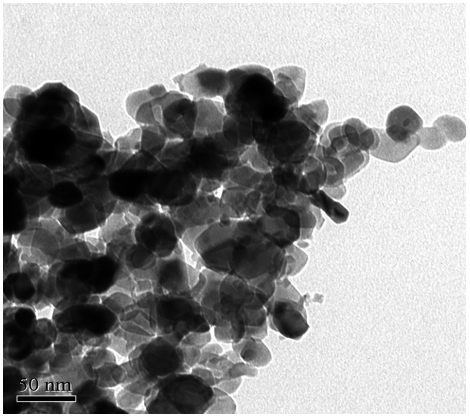

(a)

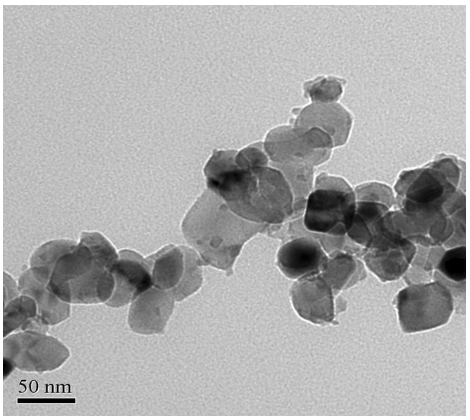

(b)

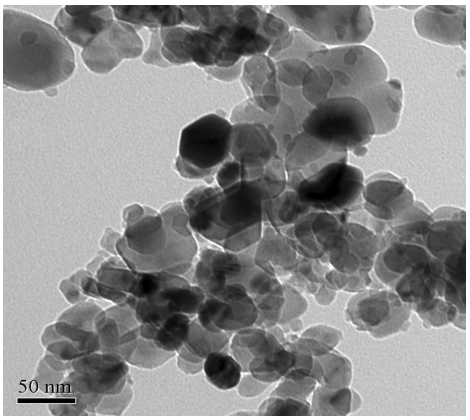

(c)

Fig. 6. TEM images of MnO_x/TiO_2 prepared from different manganese compounds: (a) MA-MnO_x/TiO_2, (b) MN-MnO_x/TiO_2, (c) MC- MnO_x/TiO_2.

641.25 eV indicating the presence of Mn^{4+} and Mn^{3+} respectively,[32,33] implying that nonstoichiometric MnO_x existed in these two samples. This might be the result of crystal defects and oxygen vacancies,[34] leading to higher activities in *o*-DCB oxidation. In addition, it can be seen that the intensity of Mn^{3+} (641.25) peak of (b) was stronger than (c), which means the content of Mn^{3+} in MN-MnO_x/TiO_2 was more than that in MC-MnO_x/TiO_2. The fact that MA-MnO_x/TiO_2 having a higher concentration of Mn but a relatively lower catalytic activity indicated that the content of Mn was not significant to the *o*-DCB oxidation. As reported by Tang,[25] the catalytic performances of the supported manganese oxide catalyst were mainly affected by the oxidation state. For *o*-DCB oxidation over MnO_x/TiO_2 catalysts, Aguero[35] demonstrated that a lower average oxidation state of manganese would enhance the performance of the catalysts. Combined with the data in Table 3 and the XRD results, a higher Mn^{3+}/Mn ratio in MN-MnO_x/TiO_2 surface, indicating a lower mean oxidation state of the manganese, could be a factor for its outperforming behavior in *o*-DCB oxidation. According to the TEM and XPS results, small particle with

Table 3. Atomic concentrations of three catalysts obtained with XPS.

	Metal content (at.%)					
Catalysts	Mn	Ti	Mn/Ti	Mn^{3+}	Mn^{4+}	Mn^{3+}/Mn
MA-MnO_x/TiO_2	5.21	14.63	0.36	3.03	2.18	0.581
MN-MnO_x/TiO_2	3.53	17.2	0.21	2.07	1.46	0.586
MC-MnO_x/TiO_2	3.48	17.26	0.20	1.58	1.90	0.454

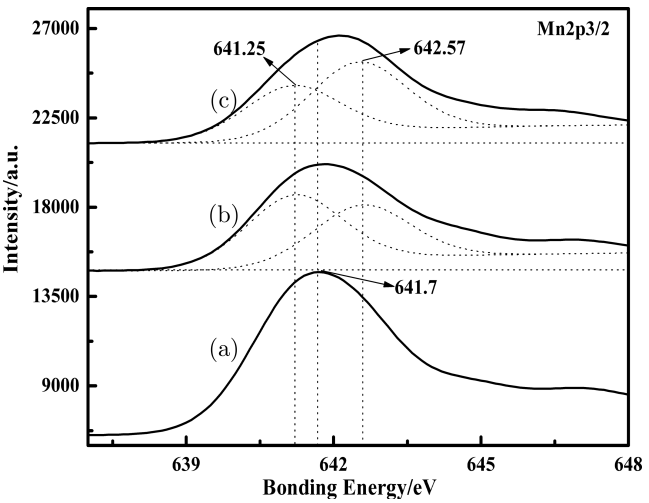

Fig. 7. Mn2p XPS spectra of MnO_x/TiO_2 prepared from different manganese compounds: (a) MA-MnO_x/TiO_2, (b) MN-MnO_x/TiO_2, (c) MC-MnO_x/TiO_2.

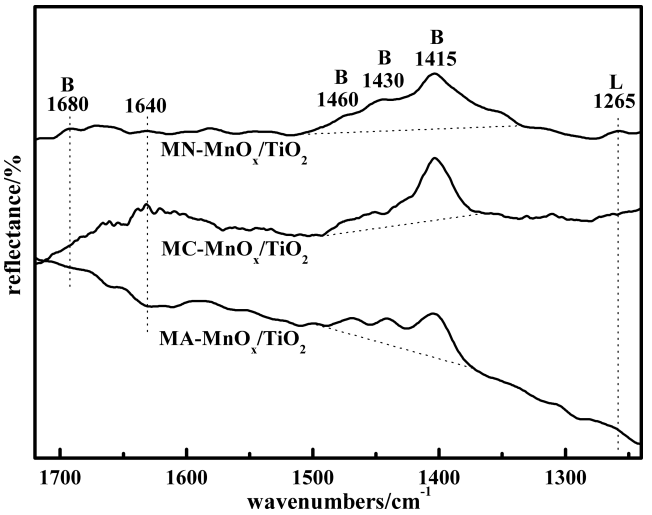

Fig. 8. DRIFTS spectra for NH_3 adsorption and desorption on MnO_x/TiO_2 prepared from different manganese compounds at room temperature.

a higher content of low average oxidation state of manganese contributed to the good catalytic performance of MN-MnO_x/TiO_2.

All the DRIFTS spectra illustrating in Fig. 8 are obtained by subtracting the spectrum of the fresh catalyst (without NH_3 adsorption at room temperature) from those received after NH_3 adsorption. As shown in Fig. 8, the peak at 1640 cm^{-1} for all the samples was assigned to the H–O bending mode of hydroxyl groups present on the surface due to moisture. In addition to this, the peaks at 1680, 1460, 1430 and 1415 cm^{-1} were attributed to the symmetric or asymmetric bending vibration of NH_4^+ formatting on Brönsted acid sites (B-sites), whereas the symmetric and asymmetric bending vibration of N–H in NH_3 coordinated to Lewis acid sites (L-sites) band markedly appeared at 1260 cm^{-1}[15]. Both the Brönsted and L-sites are beneficial for *o*-DCB remove. As shown by the spectra, it can be observed obviously that the Brönsted acid sites of MN-MnO_x/TiO_2 were the strongest in all samples. Besides that, the adsorption of NH_3 on MN-MnO_x/TiO_2, which attributed to the L-site, was stronger and sharper than that on the other samples. The reason for this may be because that the highly dispersed Mn^{3+} active sites on the MN-MnO_x/TiO_2 sample caused a better adsorption intensity of coordinated-NH_3. Combined with the IR spectra obtained after NH_3 adsorption experiment, we can conclude that the total amount of Brönsted and Lewis acid of MN-MnO_x/TiO_2 was the highest of all. Accordingly, it was suggested that the abundant Brönsted and strong Lewis site generated by more dispersed Mn^{3+} were responsible for the excellent catalytic activity of MN-MnO_x/TiO_2 for *o*-DCB. Therefore, for all the prepared MnO_x/TiO_2 composites, the catalytic efficiency was affected not only by the phase of TiO_2 and the kind of MnO_x, but also by the acidity.

3.3. *Proposed reaction model from o-DCB oxidation over MN-MnO_x/TiO_2 catalyst*

A different mechanism of 1,2-dichlorobenzene oxidation was proposed to explain the degradation of this compound over catalyst.[35] The ability of giving proton H and capturing the lone pair electrons of catalyst is characterized by the Brönsted and Lewis acidity respectively. So, some studies proved that the Brönsted and Lewis acidity were found to be a very important parameter to control the degradation of the chlorinated compounds. Thus, the results collected in FTIR and catalytic testing suggest a strong correlation between number and type of acid sites and activity to 1,2-dichorobenzene: The higher the Brönsted and Lewis acid sites, the greater the catalytic oxidation to *o*-DCB. Based on the above analysis, a possible reaction model from *o*-DCB oxidation over MN-MnO_x/TiO_2 catalyst was suggested in Fig. 9.

A mount of surface Brönsted and strong Lewis site generated by more dispersed Mn^{3+} existed in MnO_x/TiO_2 catalyst prepared from MN. When the reactants were in contacted with the catalyst, the amount of *o*-DCB may be reduced by the adsorption and oxidation of catalyst. For the adsorption, the lone pair electrons of Cl was captured by Lewis site first, making nucleophilic attack on the chlorine position, that was proposed by many authors.[36] For the oxidation, as reported by Taralunga,[37] the *o*-DCB molecule could directly react with the protonic Brönsted acid site, giving HCl, and eventually break down under the action of oxygen after several reactions. Though the specific mechanism is not yet clear, further investigation on the mechanism of *o*-DCB total oxidation over MnO_x/TiO_2 will be preceded. Then, we will perform the work to enhance the lifetime and the catalytic activity of MnO_x/TiO_2 preferentially in future.

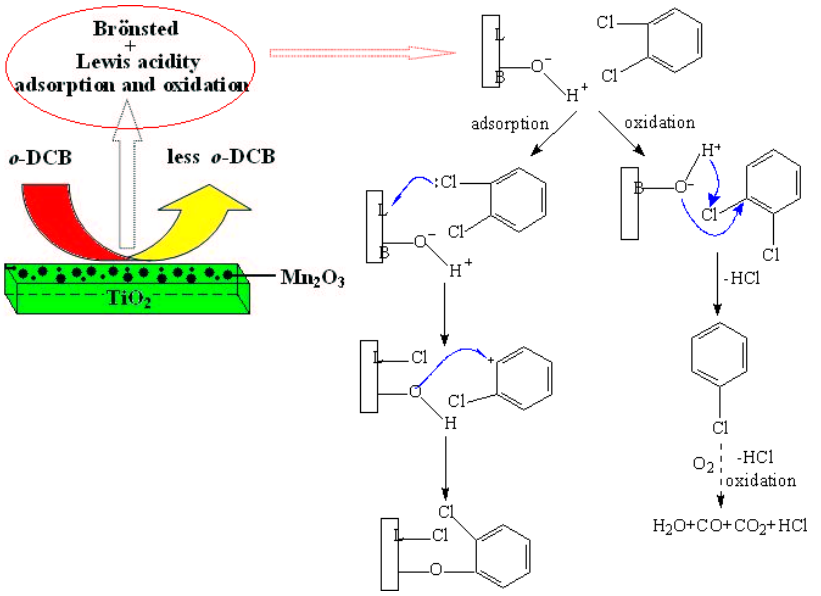

Fig. 9. A possible reaction model from *o*-DCB oxidation over MN-MnO_x/TiO_2.

4. Conclusions

Catalysts based on MnO_x/TiO_2 were prepared from three different manganese compounds. Among the catalysts, MN-MnO_x/TiO_2 with the ratio of $Mn/Ti = 1:4$ and calcination temperature 500°C showed the highest catalytic activity for *o*-DCB oxidation removal. The different surface manganese oxides yielded from different raw materials, which were suggested by the XRD and TG-DTA. It was also found that the combined TiO_2 phases of anatase and rutile will be a good carrier for the dispersion of manganese oxides. Meanwhile, the different surface Mn^{3+} concentrations and acidity of catalysts were suggested by the XPS and FTIR with adsorption of NH_3. It is concluded that the highest activity of MN-MnO_x/TiO_2 catalyst was due to more surface Mn_2O_3 species and stronger Brönsted and Lewis acidity.

Acknowledgment

Financial support of this research by the National Key Technology R&D Program in the 11th Five year Plan of China, Grant No. 2008BAC32B05-3 is gratefully acknowledged.

References

1. F. Bertinchamps, C. Gregoire and E. M. Gaigneaux, *Appl. Catal. B*: *Environ.* **1–2**, 66 (2006).
2. P. S. Kulkarni, J. G. Crespo and C. A. M. Afonso, *Environ. Int.* **1**, 34 (2008).
3. M. H. Sean and L. L. Aylward, *Regulatory Toxicol. Pharmacol.* **37**, (2003).
4. G. McKay, *Chem. Eng. J.* **3**, 86 (2002).
5. P. Liljelind, J. Unsworth, O. Maaskant and S. Marklund, *Chemosphere* **5–7**, 42 (2001).
6. A. Buekens and H. Huang, *J. Hazardous Mater.* **1**, 62 (1998).
7. A. Khaleel and A. Al-Nayli, *Appl. Catal. B*: *Environ.* **1–2**, 80 (2008).
8. S.-H. Hsu, C.-S. Huang, T.-W. Chung and S. Gao, *J. Taiwan Instit. Chem. Eng.* **5**, 45 (2014).
9. H. C. Wang, H. S. Liang and M. B. Chang, *J. Hazardous Mater.* **2–3**, 186 (2011).
10. R. Chen, D. Jin, H. Yang, Z. Ma, F. Liu and X. Zhang, *Catal Lett.* **11**, 143 (2013).
11. Y. Liu, M. Luo, Z. Wei, Q. Xin, P. Ying and C. Li, *Appl. Catal. B*: *Environ.* **1**, 29 (2001).
12. F. Kapteijn, L. Singoredjo, A. Andreini and J. A. Moulijn, *Appl. Catal. B*: *Environ.* **2–3**, 3 (1994).
13. A. Wollner, F. Lange, H. Schmelz and H. Knozinger, *Appl. Catal. A*: *General* **2**, 94 (1993).
14. Z. Wu, R. Jin, Y. Liu and H. Wang, *Catal. Commun.* **13**, 9 (2008).
15. L.-C. Wang, Q. Liu, X.-S. Huangm, Y.-M. Liu, Y. Cao and K.-N. Fan, *Appl. Catal. B*: *Environ.* **1–2**, 88 (2009).
16. C. Lahousse, A. Bernier, E. Gaigneaux, P. Ruiz, P. Grange, B. Delmon, R. K. S. T. O. A. M. G. Grasselli and J. E. Lyons, *Studies in Surface Science and Catalysis* **110**, 777 (1997).

17. C. Lahousse, A. Bernier, P. Grange, B. Delmon, P. Papaefthimiou, T. Ioannides and X. Verykios, *J. Catal.* **1**, 178 (1998).
18. H. G. Stenger Jr., G. E. Buzan and J. M. Berty, *Appl. Catal. B*: *Environ.* **1**, 2 (1993).
19. J. M. Berty, H. G. Stenger Jr., G. E. Buzan and K. Hu, Oxidation and removal of chlorinated hydrocarbons, *Studies Surface Sci. Catal.* **75**, 1571 (1993).
20. B. Jiang, Y. Liu and Z. Wu, *J. Hazardous Mater.* **2**–**3**, 162 (2009).
21. B. Jiang, Dissertation Submitted to Zhejiang University for the Degree of Doctor of Philosophy, Vol. 7 (2008).
22. F. Kapteijn, A. D. Vanlangeveld, J. A. Moulijn, A. Andreini, M. A. Vuurman, A. M. Turek, J. M. Jehng and I. E. Wachs, *J. Catal.* **1**, 150 (1994).
23. D. A. Pena, B. S. Uphade and P. G. Smirniotis, *J. Catal.* **2**, 221 (2004).
24. J. Li, J. Chen, R. Ke, C. Luo and J. Hao, *Catal. Commun.* **12**, 8 (2007).
25. X. Tang, J. Hao, W. Xu and J. Li, *Catal. Commun.* **3**, 8 (2007).
26. Sachtleben Chemie GmbH. Hombikat UV 100 from Sachtleben Chemie. http://www.shzewen.com.cn/zewen/product/.
27. W. Tian, X. Fan, H. Yang and X. Zhang, *J. Hazardous Mater.* **1**–**3**, 177 (2010).
28. C. Su, B. Y. Hong and C. M. Tseng, *Catal. Today* **3**, 96 (2004).
29. G. A. F. José Luis Contreras, Sintering — Methods and Products, www.intechopen.com.
30. S. Yamazoe, T. Okumura, K. Teramura and T. Tanaka, *Catal. Today* **3**–**4**, 111 (2006).
31. Y. Hasegawa, K. Fukumoto, T. Ishima, H. Yamamoto, M. Sano and T. Miyake, *Appl. Catal. B*: *Environ.* **3**–**4**, 89 (2009).
32. A. S. Reddy, C. S. Gopinath and S. Chilukuri, *J. Catal.* **2**, 243 (2006).
33. E. Lopez-Navarrete, A. Caballero, A. R. Gonzalez-Elipe and M. Ocana, *J. Eur. Ceramic Soc.* **10**–**11**, 24 (2004).
34. D. Yu, Y. Liu and Z. Wu, *Catal. Commun.* **8**, 11 (2010).
35. F. N. Aguero, A. Scian, B. P. Barbero and L. E. Cadus, *Catal. Today* **133**–**135**, (2008).
36. J. Lichtenberger and M. D. Amiridis, *J. Catal.* **2**, 223 (2004).
37. M. Taralunga, J. Mijoin and P. Magnoux, *Catal. Commun.* **3**, 7 (2006).